Electromagnetic-thermal model of a millimeter-wave heat exchanger based on an AlN:Mo susceptor

Petra Kumi, Stephanie A. Martin and Vadim V. Yakovlev
Department of Mathematical Sciences, Worcester Polytechnic Institute, Worcester, Massachusetts, USA

Martin S. Hilario and Brad W. Hoff
Air Force Research Laboratory Directed Energy Directorate, Albuquerque, New Mexico, USA, and

Ian M. Rittersdorf
US Naval Research Laboratory, Washington, District of Columbia, USA

Received 1 July 2019
Revised 29 October 2019
Accepted 20 November 2019

Abstract

Purpose – The paper introduces and illustrates the use of numerical models for the simulation of electromagnetic and thermal processes in an absorbing ceramic layer (susceptor) of a new millimeter-wave (MMW) heat exchanger. The purpose of this study is to better understand interaction between the MMW field and the susceptor, choose the composition of the ceramic material and help design the physical prototype of the device.

Design/methodology/approach – A simplified version of the heat exchanger comprises a rectangular block of an aluminum nitride (AlN) doped with molybdenum (Mo) that is backed by a thin metal plate and irradiated by a plane MMW. The coupled electromagnetic-thermal problem is solved by the finite-difference time-domain (FDTD) technique implemented in QuickWave. The FDTD model is verified by solving the related electromagnetic problem by the finite element simulator COMSOL Multiphysics. The computation of dissipated power and temperature is based on experimental data on temperature-dependent dielectric constant, loss factor, specific heat and thermal conductivity of the AlN:Mo composite. The non-uniformity of patterns of dissipated power and temperature is quantified via standard-deviation-based metrics.

Findings – It is shown that with the power density of the plane wave on the block's front face of 1.0 W/mm^2, at 95 GHz, 10 × 10 × 10-mm blocks with Mo = 0.25 – 4% can be heated up to 1,000 °C for 60-100 *s* depending on Mo content. The uniformity of the temperature field is exceptionally high – in the course of the heating, temperature is evenly distributed through the entire volume and, in particular, on the back surface of the block. The composite producing the highest level of total dissipated power is found to have Mo concentration of approximately 3%.

Research limitations/implications – In the electromagnetic model, the heating of the AlN:Mo samples is characterized by the volumetric patterns of density of dissipated power for the dielectric constant and the loss factor corresponding to different temperatures of the process. The coupled model is run as an iterative procedure in which electromagnetic and thermal material parameters are upgraded in every cell after each heating time step; the process is then represented by a series of thermal patterns showing time evolution of the temperature field.

The authors are grateful for the support from the the Air Force Research Laboratory, Leidos, Inc., Grant No P010200226. The work of P. Kumi was supported by the 2018 WPI Summer Undergraduate Research Fellowship (SURF). B.W. Hoff and M.S. Hilario were funded by the Air Force Office of Scientific Research under FA9550-17RDCOR449 and by the Operational Energy Capability Improvement Fund (OECIF). I. Rittersdorf was supported by OECIF.

COMPEL - The international journal for computation and mathematics in electrical and electronic engineering
0332-1649
DOI 10.1108/COMPEL-07-2019-0271

Practical implications – Determination of practical dimensions of the MMW heat exchanger and identification of material composition of the susceptor that make operations of the device energy efficient in the required temperature regime require and expensive experimentation. Measurement of heat distribution on the ceramic-metal interface is a practically challenging task. The reported model is meant to be a tool assisting in development of the concept and supporting system design of the new MMW heat exchanger.

Originality/value – While exploitation of a finite element model (e.g. in COMSOL Multiphysics environment) of the scenario in question would require excessive computational resources, the reported FDTD model shows operational capabilities of solving the coupled problem in the temperature range from 20°C to 1,000°C within a few hours on a Windows 10 workstation. The model is open for further development to serve in the ongoing support of the system design aiming to ease the related experimental studies.

Keywords Multiphysics, Thermal analysis, Finite difference time-domain analysis, Wireless power transfer, Dielectric properties

Paper type Research paper

1. Introduction

Electromagnetic (EM) heating has been commonly used in a variety of applications in food engineering, chemistry and materials science (Datta and Anartheswaran, 2001; Willert-Porada, 2006; Feher, 2009; Leadbeater, 2010). This phenomenon is also in the core of the recently introduced devices for solar energy collectors (Jamar *et al.*, 2016) and microwave thermal thrusters (Parkin *et al.*, 2004; Komurasaki and Tabata, 2018) as well as in EM heat exchangers (HX) for ground-to-ground millimeter-wave (MMW) power beaming applications (Komerath and Kar, 2012; Etinger *et al.*, 2017; Jawdat *et al.*, 2017; Hoff *et al.*, 2018). As the latter devices are intended for the conversion of EM energy into heat (and subsequently into useful mechanical work), their functionality strongly depends on the combined effects of EM, heat transfer and fluid flow phenomena. This indicates that the interactions of the MMW field with a ceramic element of a HX should be well understood for effectively using EM energy, controllably heating the material and transferring heat to another medium (fluid). The design of efficient MMW HX is therefore expected to benefit from multiphysics modeling capable of adequately simulating all essential effects (Mohekar *et al.*, 2018a; Mohekar *et al.*, 2018b; Gaone *et al.*, 2019; Mohekar *et al.*, 2019a; Mohekar *et al.*, 2019b).

A new type of MMW-powered HX currently under development comprises an assembly of ceramic tiles and a metal baseplate at their back surfaces that contains channels with fluid flow (Figure 1). Because of dielectric losses, the EM power of the incident wave is dissipated in the ceramic blocks, and the induced thermal field heats the attached baseplate (and thus the fluid flowing in the channels). In an efficient device, the ceramic material used in the tiles should possess special EM and thermal properties such as high loss factor, high thermal conductivity, an ability to withstand high temperatures (up to 1000-1500 °C) and

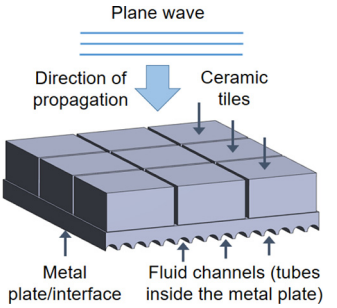

Figure 1.
Conceptual drawing of a section of a MMW-powered HX

high thermal gradients. While from some initial experiments a particular material may appear generally suitable, determination of device's practical dimensions and material composition that make operations of the device energy efficient in the required temperature regime would require extensive and expensive experimentation. Moreover, distribution of the heat on the ceramic-metal interface is of great importance, but measurement of temperature patterns there is a challenging task. Comprehensive modeling exploring the EM and thermal processes with the use of appropriate model of a MMW HX and suggesting the choice of parameters of its physical prototype is therefore in high demand.

In this paper, using EM and coupled EM-thermal modeling performed in QuickWave™ environment, we study the process of heating of a rectangular block of an aluminum nitride-molybdenum composite (AlN:Mo) by a normally incident plane MMW. The back surface of the block is attached to a thin metal plate. A variety of material compositions are considered by analyzing the samples with different Mo concentration (by volume). The experimental data on temperature-dependent characteristics of EM (at 95 GHz) and thermal material parameters of the specific AlN:Mo formulations are approximated and extrapolated to be used as input data for the coupled EM-thermal simulation. In the framework of EM modeling, the heating of the ceramic samples is characterized by the volumetric patterns of density of dissipated power for the dielectric constant and the loss factor corresponding to different temperatures of the process. The coupled modeling is run in the range from room temperature (20°C) to 1,000°C as an iterative procedure in which EM and thermal material parameters are upgraded in every cell after each heating time step. In this case, the process is represented by a series of temperature patterns showing time evolution of the thermal field. All faces of the composite sample are considered thermally insulated. The temperature fields are shown to be exceptionally uniform for all concentrations of Mo and throughout the entire temperature range. In terms of the level of absorbed power, the composite with Mo ~ 3 per cent appears to provide the highest energy efficiency and, as such, is recommended for use in a physical prototype.

2. Computational scenario and input data

Aiming to help design the first physical prototype of a MMW HX, we report here a computer model capable of simulating EM and EM-induced thermal processes in a single ceramic block of the system in Figure 1 that is irradiated by a plane wave and attached to a thin metal plate (Figure 2). the ultimate goal of the computational experiments is to determine a composition of the composite material that absorbs maximum MMW power and, at the same time, produces satisfactorily uniform temperature distribution on the back surface.

2.1 Ceramic composite

The concept of a MMW HX requires the absorbing ceramic to possess particularly high thermal conductivity k (a thermal material parameter) and the loss factor ε'' (an EM

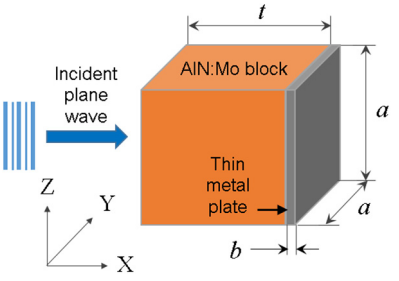

Figure 2.
3D views of the considered computational scenario

material parameter, an imaginary part of complex permittivity $\varepsilon = \varepsilon' - i\varepsilon''$, where ε' is dielectric constant). High k is expected to help disperse the heat potentially concentrated in some areas (hot spots) because of the non-uniformity of EM heating and elevate the heat transfer to the adjacent metal baseplate. High ε'' intends for the strong absorption of EM energy and thus its efficient conversion into the heat.

In this work, the requirement for high thermal conductivity is responded by selecting aluminum nitride (AlN) as a ceramic matrix. Furthermore, it was found that small doses of Mo doping are capable of substantial (up to two orders of magnitude) increase of the loss factor of the AlN:Mo composite (Hoff *et al.*, 2019a, 2019b). We therefore investigate what level of energy efficiency and heating uniformity can be achieved by examining the behavior of the system in Figure 2 for different levels of Mo content (from 0.25 to 4 per cent by volume) in the temperature range from 20 to 1,000 °C. (The considered ceramic composite also contains some yttrium and trace carbon as sintering additives).

2.2 Electromagnetic material parameters

EM and thermal material parameters of ceramics are known to be temperature-dependent, so the functionality of related devices may be fairly different at different temperatures (Ayappa *et al.*, 1991; Yakovlev *et al.*, 2011; Hossan and Dutta, 2012; Kashimura *et al.*, 2016). Temperature characteristics of ε' and ε'' of the considered AlN:Mo composites were obtained with a dedicated apparatus for a free space dielectric measurement (Hilario *et al.*, 2017; Hilario *et al.*, 2019; Hoff *et al.*, 2019b) at 95 GHz for temperatures T of up to 500-600°C. The measurements were carried out for six samples with Mo = 0.25, 0.5, 1.0, 2.0, 3.0 and 4.0 per cent.

It is seen from Figure 3 that experimental points for both dielectric constant and the loss factor form almost linearly increasing functions of temperature for all Mo concentrations. As expected, the values of ε'' go up with increase of the doping; with Mo = 4 per cent, the loss factor is approximately 30 times higher than in the absence of the doping. However, as it turned out, ε' also increases with higher percentage of molybdenum content: for Mo = 4 per cent, it is approximately 1.5 times larger compared to Mo = 0.25 per cent. This suggests that MMW heating of the composites with different Mo contents may occur very differently because of different distributions of the electric field.

The experimental points were interpolated to obtain linear functions approximating temperature characteristics of dielectric constant and the loss factor for all material compositions as follows:

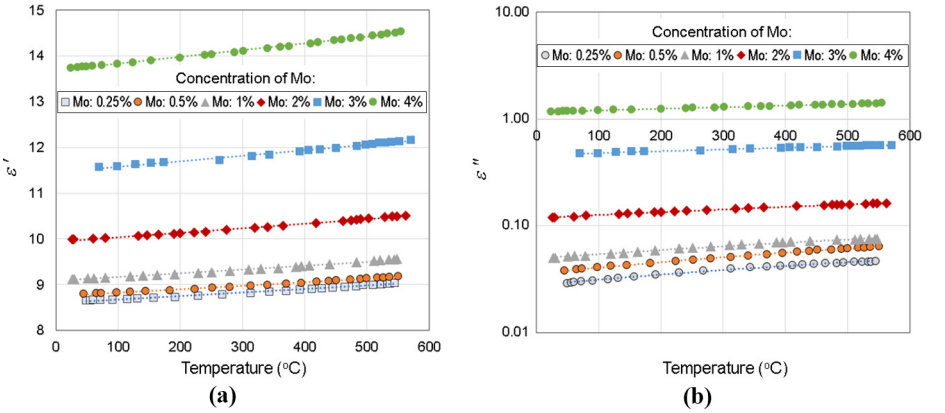

Figure 3.
Measured points and linearly approximated temperature characteristics of dielectric constant ε' (a) and the loss factor ε'' (b) of six AlN:Mo samples with different concentrations of Mo

$$\varepsilon' = \begin{cases} 0.0008T + 8.5979 \ (R^2 = 0.992) \ \text{for Mo} = 0.25\% \\ 0.0008T + 8.7424 \ (R^2 = 0.994) \ \text{for Mo} = 0.5\% \\ 0.0008T + 9.0785 \ (R^2 = 0.992) \ \text{for Mo} = 1.0\% \\ 0.0010T + 9.9373 \ (R^2 = 0.995) \ \text{for Mo} = 2.0\% \\ 0.0012T + 11.458 \ (R^2 = 0.989) \ \text{for Mo} = 3.0\% \\ 0.0015T + 13.681 \ (R^2 = 0.996) \ \text{for Mo} = 4.0\% \end{cases} \quad (1)$$

$$\varepsilon'' = \begin{cases} 0.00004T + 0.0277 \ (R^2 = 0.994) \ \text{for Mo} = 0.25\% \\ 0.00005T + 0.0353 \ (R^2 = 0.998) \ \text{for Mo} = 0.5\% \\ 0.00005T + 0.0491 \ (R^2 = 0.994) \ \text{for Mo} = 1.0\% \\ 0.00005T + 0.1181 \ (R^2 = 0.999) \ \text{for Mo} = 2.0\% \\ 0.0002T + 0.4613 \ (R^2 = 0.995) \ \text{for Mo} = 3.0\% \\ 0.0004T + 0.1589 \ (R^2 = 0.999) \ \text{for Mo} = 4.0\% \end{cases} \quad (2)$$

The values of the correlation coefficient R^2 in (1)-(2) show that the interpolations are indeed very close to linear functions.

2.3 Thermal material parameters

Density ρ of the AlN:Mo samples with variable Mo content was measured in Hoff *et al.* (2019a) by the Archimedes method using methyl ethyl ketone as the fluid. The values of ρ were found to be forming a nearly linear function of Mo concentration. Using this function, in this paper, the density values are considered as:

$$\rho \left[\frac{g}{cm^3}\right] = \begin{cases} 3.32 \ \text{for Mo} = 0.25\% \\ 3.33 \ \text{for Mo} = 0.5\% \\ 3.37 \ \text{for Mo} = 1.0\% \\ 3.44 \ \text{for Mo} = 2.0\% \\ 3.50 \ \text{for Mo} = 3.0\% \\ 3.57 \ \text{for Mo} = 4.0\% \end{cases} \quad (3)$$

and assumed to be temperature-independent.

Data on temperature characteristics of the specific heat capacity C_p of all six AlN:Mo composites in the interval from 100 to 1,000°C was taken from Hoff *et al.* (2019a), as shown in Figure 4(a). In the referenced paper, the points were calculated, using the mixture models, for six particular temperatures; to verify the calculations, samples of three compositions (Mo = 0.25, 0.5, and 1.0 per cent) were measured using differential scanning calorimetry in which uncertainty of C_p values was within 5 per cent in the interval from 30 to 600°C. While the data points show no strong dependence on Mo concentration, it is seen that the heat capacity significantly increases with temperature.

To obtain functions approximating characteristics of C_p for all six samples in the entire temperature range, the experimental points in Figure 4(a) were approximated by polynomials of order 4 as follows:

$$C_P\left[\frac{J}{kgK}\right] = \begin{cases} -10^{-9}T^4 + 3\cdot 10^{-6}T^3 - 0.0033T^2 + 1.8372T + 666.21 \ (R^2 = 1.0) \text{ for Mo} = 0.25\% \\ -10^{-9}T^4 + 3\cdot 10^{-6}T^3 - 0.0032T^2 + 1.7904T + 669.15 \ (R^2 = 1.0) \text{ for Mo} = 0.5\% \\ -10^{-9}T^4 + 3\cdot 10^{-6}T^3 - 0.0031T^2 + 1.7621T + 657.7 \ (R^2 = 1.0) \text{ for Mo} = 1.0\% \\ -10^{-9}T^4 + 3\cdot 10^{-6}T^3 - 0.0031T^2 + 1.7351T + 647.3 \ (R^2 = 1.0) \text{ for Mo} = 2.0\% \\ -9\cdot 10^{-10}T^4 + 3\cdot 10^{-6}T^3 - 0.003T^2 + 1.6797T + 635.99 \ (R^2 = 1.0) \text{ for Mo} = 3.0\% \\ -10^{-9}T^4 + 3\cdot 10^{-6}T^3 - 0.0031T^2 + 1.7011T + 625.41 \ (R^2 = 1.0) \text{ for Mo} = 4.0\% \end{cases} \quad (4)$$

Data on temperature characteristics of thermal conductivity k of all six materials in the interval from 100 to 1,000°C was also taken from Hoff *et al.* (2019a); the data points are shown in Figure 4(b). In the referenced paper, the values of k were calculated (with uncertainty estimated to be within 10 per cent) from experimental data on thermal diffusivity, which was measured by the laser flash method. Moreover, the data points show no strong dependence on Mo concentration, but reveal a strong decrease of thermal conductivity with temperature.

Functions approximating characteristics of k were obtained by approximating the data points by polynomials of orders 3 and 4 as follows:

$$k\left[\frac{W}{mK}\right] = \begin{cases} -3\cdot 10^{-7}T^3 + 0.0006T^2 - 0.4104T + 148.26 \ (R^2 = 0.997) \text{ for Mo} = 0.25\% \\ -10^{-8}T^3 + 0.0001T^2 - 0.2163T + 128.43 \ (R^2 = 1.0) \text{ for Mo} = 0.5\% \\ 6\cdot 10^{-10}T^4 - 10^{-6}T^3 + 0.0011T^2 - 0.4488T + 138.58 \ (R^2 = 1.0) \text{ for Mo} = 1.0\% \\ 3\cdot 10^{-10}T^4 - 8\cdot 10^{-7}T^3 + 0.0008T^2 - 0.4052T + 145.34 \ (R^2 = 1.0) \text{ for Mo} = 2.0\% \\ 5\cdot 10^{-10}T^4 - 10^{-6}T^3 + 0.001T^2 - 0.466T + 146.3 \ (R^2 = 1.0) \text{ for Mo} = 3.0\% \\ 4\cdot 10^{-10}T^4 - 10^{-6}T^3 + 0.0009T^2 - 0.4006T + 142.2 \ (R^2 = 0.997) \text{ for Mo} = 4.0\% \end{cases} \quad (5)$$

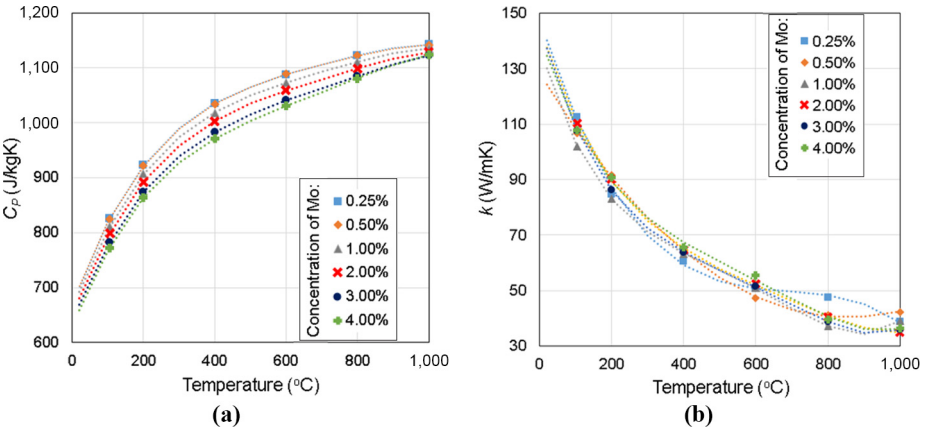

Figure 4.
Measured points and approximated temperature characteristics of specific heat C_p and thermal conductivity k of the AlN:Mo sample with different concentrations of Mo

2.4 The model

Computations were carried out for the scenario shown in Figure 2 for the following parameters: the AlN:Mo block: cross-sectional dimension a = 10 mm and thickness t = 8-12 mm; thickness of the metal plate b = 1 mm; frequency of the incident plane wave f = 95 GHz and the power density of incoming irradiation at the front face of the composite block P_{din} = 0.3 and 1.0 W/mm^2.

3. Computational techniques

3.1 Electromagnetic and thermal problems

The process of MMW heating of the AlN:Mo block with the thin metal plate adjacent to its back surface was studied with EM and EM-thermal (coupled) models. The latter mimics the time evolution of the MMW-induced temperature field under the determined temperature-dependent EM and thermal material parameters. Both underlying problems are numerically solved by a 3D finite-difference time-domain (FDTD) technique.

The models were built in the environment of the FDTD solver QuickWave^{TM} (QW) that includes its thermal unit QW-BHM^{TM} (QuickWave, 1998-2019). The procedure used for coupling the two solvers is similar to the ones outlined in Kopyt and Celuch (2007), Celuch and Kopyt (2009), Koutchma and Yakovlev (2010) and Yakovlev *et al.* (2011). The EM and thermal solvers operate as parts of an iterative procedure in which a steady state solution of the EM problem becomes an input for the thermal problem, and, in the repeated runs of the EM solver, material parameters are upgraded in every cell in accordance with the temperature field outputted from the thermal solver. The latter determines temperature distribution induced after each heating time step Δt; N steps are needed to reach maximum temperature of the process.

The corresponding polynomial approximations (1)-(5) were used to generate the values of ε', ε'', C_p, and k at 20, 100, 200, …, 1,000°C as tabulated input data for the EM-thermal model. The step of 100°C is selected to guarantee adequate representations of temperature characteristics of all material parameters.

The 10 × 10 × 10 mm AlN:Mo block (adjacent to the 1 mm metal plate) is surrounded by the 18 × 13 × 13 mm plane wave box with one 13 × 13 mm face responsible for sinusoidal excitation of the incident field.

This box is situated inside the 24 × 19 × 19 mm box imitating the Mur with superabsorption boundary condition (Mur, 1981; Yu, 2009; QuickWave, 1998-2019), as shown in Figure 5.

To satisfy the Courant stability criterion and minimize computational resources, the scenario is discretized with the mesh with maximum cell sizes of 0.29 (in air) and from 0.075

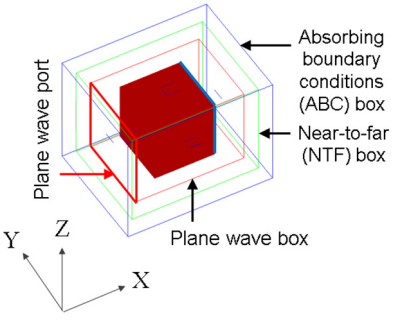

Figure 5.
3D views of the structure of the model

to 0.095 mm (in the media, in accordance with dielectric constants of the composites with Mo = 4 and 0.25 per cent, respectively). Depending on the Mo content, the model comprises 6.2-10.8 million cells (593 and 1,025 MB RAM, respectively).

In this study, simulations are performed on a Windows 10 workstation with two Intel Xeon Gold 5120 processors with a base/peak frequency of 2.2/3.2 GHz (each having 14 cores and supporting 28 threads), the GPU NVIDIA Quadro P5000 and 1 TB RAM.

The EM model computes patterns of density of dissipated power (P_d) that is dispersed in the volume of the composite because of dielectric losses. These patterns are visually identical to temperature distributions at the initial moment of heat dissipation ($t = 0$) because of thermal conductivity.

The thermal problem is solved on the same mesh under Neumann (adiabatic) boundary conditions on all (ceramic-air and ceramic-metal) interfaces.

3.2 Benchmark problem

While experimental validation is not possible et, the output of the developed FDTD model can be compared with the one generated by another numerical solver. The results of the EM component of the coupled FDTD model are compared to the output of a finite element (FE) EM frequency-domain model built in COMSOL Multiphyscis (1998-2019). Application of a COMSOL model directly to our problem of interest would require impractical computational resources (in terms of both RAM and CPU time). For this reason, both FDTD and FE models are applied to the structure in Figure 2 in the microwave frequency range with geometrical and material parameters listed in Table I. The ceramic block is assumed to be made of zirconia; its complex permittivity at 2.45 GHz is taken from Yakovlev *et al.* (2011).

For the test problem, the mesh in the FDTD model is built with maximum 6 and 2 mm cell sizes in air and zirconia, respectively; for the ABC box of 240 × 190 × 190 mm, this makes the total number of cells to be 152,880. This FDTD discretization indicates the use of more than 20 cells per wavelength. Aiming to reach high accuracy of simulation, in the FE model for the domain of the same size, the 3 D mesh of quadratic tetrahedral elements is built under the condition of 10 elements (Salvi *et al.*, 2010; Salvi *et al.*, 2011) that exceeds the FE convention of 6 elements (Langer *et al.*, 2017); total number of elements is 288,797.

2D distributions of dissipated power in the ceramic block that are produced by both models are shown in Figure 6. As the patterns appear nearly identical, this gives us an additional degree of confidence in the developed FDTD model.

Table I.
Parameters of the test scenario for validation of the FDTD model

Frequency (GHz)	Power density (W/m^2)	Ceramic block (mm)	Metal plate (mm)	ε'	ε''
2.45	70.15	100 × 100 × 100	100 × 100 × 10	6.69	0.19

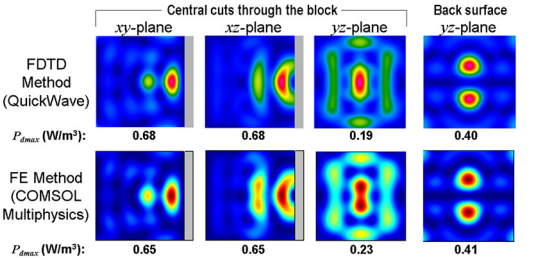

Figure 6.
Patterns of density of dissipated power in the test scenario (Table I) along with corresponding maximum values P_{dmax}

3.3 Metrics of heating uniformity and energy efficiency

Sufficient homogeneity of heating of the ceramic block is one of the required features of a MMW HX. To constructively evaluate the levels of uniformity, we use the metrics for quantitative characterization of patterns induced by EM heating that are outlined in Moon and Yakovlev (2018), Kumi and Yakovlev (2019). For patterns of dissipated power, which is the output of the EM model, the metric is the ratio of the standard deviation σ of the P_d values in all FDTD cells in the block from the average value and μ is the mean value of P_d:

$$\lambda_P = \frac{\sigma}{\mu} \tag{6}$$

In the coupled model, temperature field is computed after each EM-thermal iteration, and a sequence of temperature patterns can be seen as representing evolution of the temperature field in time. While each individual temperature distribution can be evaluated with formula (6), n patterns ($n \leq N$) are necessary to characterize the process. Therefore, the temperature uniformity in the MMW heating process can be characterized with the use of the formula:

$$\lambda_T = \frac{1}{n}\sum_{i=1}^{n}\frac{\sigma_i}{\mu_i} \tag{7}$$

where σ_i and μ_i represent the standard deviations and the means of temperature data points in each pattern involved in the characterization, respectively.

In the present study, the uniformity of MMW heating of the AlN:Mo block is characterized by computing λ_P and λ_T for 2 D patterns of P_d and T in the XY-, XZ- and YZ-coordinate planes. 2 D FDTD data for (6) and (7) is extracted from the dumped QW files containing 3 D matrices of P_d and T.

We also introduce the parameter:

$$\eta = \frac{\overline{P}_d}{P} \tag{8}$$

where $\overline{P}_d$ is the power dissipated in the composite material and P is the power carried by the incident wave as a measure of energy efficiency of the MMW heating process.

4. Results and discussion

Typical distributions of the density of dissipated power within the AlN:Mo block are shown in Figure 7. For T = 400 and 800°C, the patterns are computed under the assumption that the material is heated uniformly and, therefore, the values of complex permittivity at those temperatures are the same throughout the ceramic composite. Of particular interest is distribution of heat on the back surface of the block; therefore, Figure 7 shows the patterns in the last layer of the FDTD cells inside the ceramic block in the X-direction (i.e. in the YZ-plane).

It is seen that the P_d patterns are characterized by large amounts of local maxima (*hot spots*). For higher concentrations of Mo, the loss factor is higher, and the effect of attenuation within the block is clearly observed. The amount and magnitudes of those maxima spread over the 10 × 10 mm area suggests that, because of the high thermal conductivity of the AlN:Mo composites, the material may be heated sufficiently uniformly.

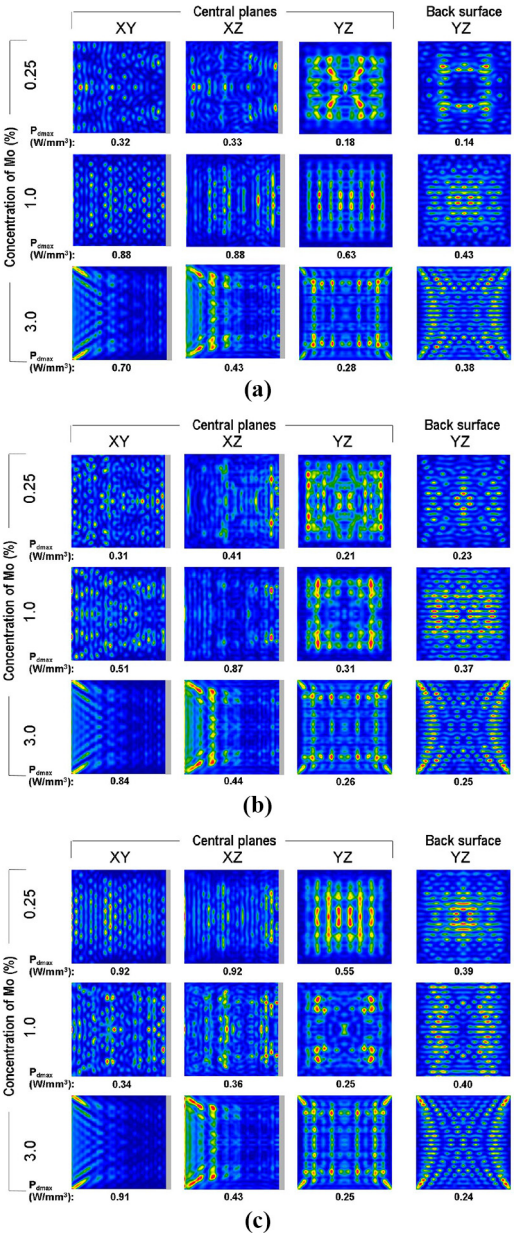

Figure 7.
Patterns of density of dissipated power in the central coordinate planes and on the back surface of the AlN:Mo block with Mo = 0.25%, 1.0% and 3.0% at $T = 20$ (a), 400 (b) and 800°C (c) along with maximum values of the power density (P_{dmax}) in each pattern; $P_{din} = 1.0$ W/mm^2; $t = 10$ mm

Temperature distributions computed by the coupled model and shown in Figure 8 show the MMW heating processes for all six AlN:Mo composites. Exceeding the anticipation suggested by Figure 7, the patterns turn out to be remarkably uniform for all compositions of the material. (This, in turn, justifies the assumption about uniformity of heating that was

used in computations of density of dissipated power in the EM model (Figure 7). Very high level of uniformity of temperature patterns is illustrated by the time characteristics of maximum and minimum temperatures in Figure 9. It is seen that the curves are almost identical; one can notice small (5-50°C) differences between $T_{\max}$ and $T_{\min}$ only in the composites with higher concentrations of Mo that are heated, because of their higher losses, most rapidly. For the composite with lowest content of Mo (0.25 per cent), the temperature of 1,000°C is reached for ~100 *s*; however, in the block made of AlN:Mo with Mo = 3-4 per cent, this level is reached for 60-65 s. For lower power density of the incoming MMW field, the heating rate is naturally much lower: when P_{din} = 0.3 W/mm^2, the composites reach the temperatures of 270-520°C, depending on the Mo contents, after 100 *s*.

A special computational test with the model without the metal plate shows that in that case the rate of heating of AlN:Mo blocks with small doping is slightly lower. This indicates that the samples with lower loss factors may experience the effect of additional heating by the wave reflected from the metal surface.

Quantitative characterizations of the heating patterns in Figures 7-8 are shown in Figure 10. While it is not easy, based on a visual inspection, to sort out the distributions of power density, formula (6) suggests that the patterns are slightly more uniform in the blocks with higher concentrations of Mo. This may be relevant to the fact that for higher loss factor less stronger peaks arise in the pattern throughout the block's volume because of stronger attenuation. Because the temperature patterns are exceptionally uniform, the values of λ_T are all very low (of the order of 10^{-4}). The increase in the curve in Figure 10(b) is consistent

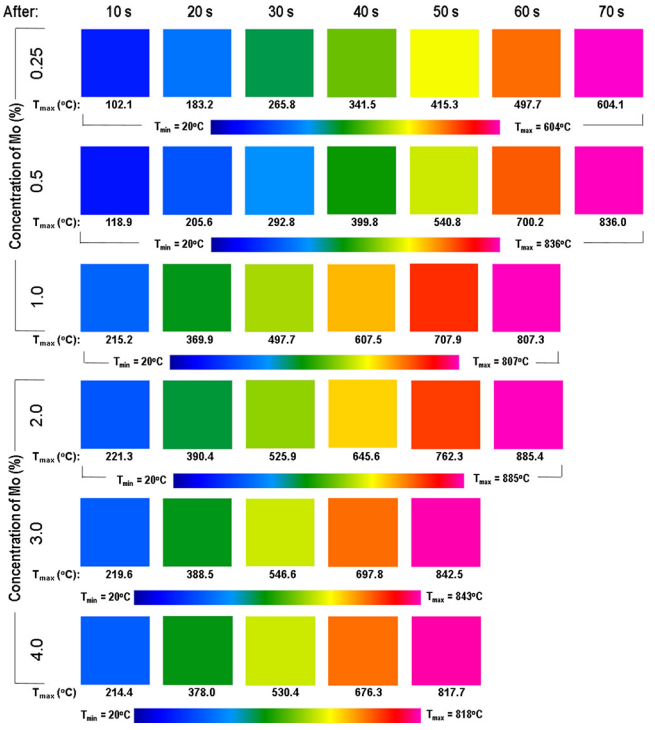

Figure 8. Temperature distributions on the back surface (YZ-plane) of the AlN:Mo block with Mo = 0.25%, 0.5%, 1.0%, 2.0%, 3.0% and 4.0% and along with maximum values of temperature (T_{max}) in each pattern. Patterns are normalized to the minimum temperature of the process (20°C); heating time steps are 5 (Mo = 0.25% and 0.5%), 2.5 (Mo = 1.0% and 2.0%), and 2.0 *s* (Mo = 3.0% and 4.0%); P_{din} = 1.0 W/mm^2; t = 10 mm

with small differences observed between the minimum and maximum temperatures in Figure 9 for the composites with higher contents of Mo.

Parameter η computed for all six Mo concentrations and the two cases of absent and present metal plate reveals a maximum energy efficiency for the AlN:Mo block with Mo near 3 per cent (Figure 11). Each point in Figure 11 corresponds to the average value of absorbed power over the temperatures 20, 200, 400, …, 1,000 °C with those temperatures represented in the EM model via corresponding values of the composite's dielectric constant and the loss factor. The results in Figure 11 may be an indication that reflection from the block with higher doping (Mo > 3 per cent) is higher than transmission (and absorption) because of higher complex permittivity. The maximum of η versus Mo characteristic near 3 per cent suggests that the composite with this level of doping may be most energy efficient material for the MMW HX analyzed in this computational study.

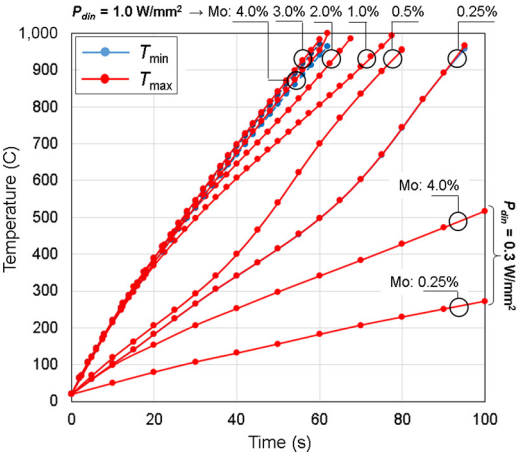

Figure 9.
Time evolution of maximum and minimum temperatures (T_{max} and T_{min}) of the MMW heated AlN: Mo blocks with different concentrations of Mo (0.25%−4%) and power densities of the incident wave (0.3 and 1.0 W/mm^2); t = 10 mm

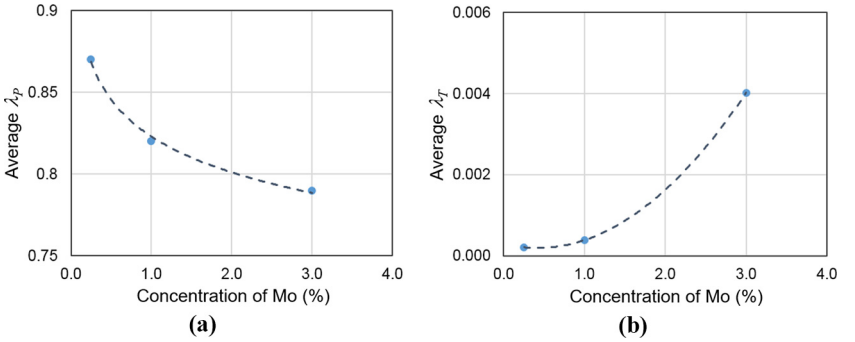

Figure 10.
Metrics of uniformity of patterns of density of dissipated power (a) and temperature (b) in Figures 7-8 as functions of Mo content: λ_P is averaged over the metrics calculated for 20, 400, and 800°C; λ_T is averaged over the metrics calculated for heating after 10, 20, . . ., 70 s

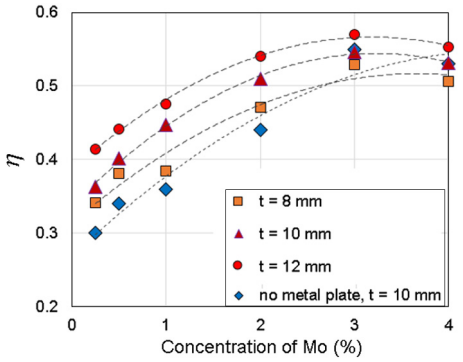

Figure 11.
Energy efficiency of the AlN:Mo block for different Mo content

5. Conclusions

The performed computational studies allow us to make the following observations. Overall, the AlN:Mo composite blocks look very attractive for the use in MMW HX of the considered structure. When the plane wave carries the power density of a practical level, 0.3-1.0 W/mm^2, the AlN:Mo blocks of $10 \times 10 \times 10 \pm 2$ mm are heated up to 1,000 C for 60-100 *s*, depending on the power and Mo content. While the patterns of density of dissipated power are characterized by multiple hot spots, the sample is heated exceptionally uniformly, and temperature is evenly distributed not only on the back surface of the block but through the entire volume. These results may be seen as clear evidence of a favorable choice of AlN:Mo for a susceptor material in the MMW HX of the considered design: high loss factor and high thermal conductivity of the composite strongly support fast and uniform heating.

While the level of uniformity is very high in samples with all concentrations of Mo, the material with 3 per cent content appears to be absorbing the most power from the incoming wave. Moreover, a preliminary conclusion made in production of the AlN:Mo composites suggests that the materials with Mo at least 3 per cent are mechanically more stable and robust. The composites of those concentrations of Mo appear to be good candidates for use in the physical prototype of a MMW-powered heat exchanger.

In the composites with low concentrations of Mo, the present metal plate makes a more notable impact on propagation of the MMW field in the considered composite block by producing the reflected wave making additional contribution to the resulting temperature field.

The developed model appears to be viable. While the development and exploitation of a finite-element model (e.g. in COMSOL Multiphysics^{TM} environment) of the scenario in question seems to be impractical, the FDTD model implemented in QuickWave^{TM} shows operational capabilities of solving the coupled problem in the temperature range from 20 to 1000°C with relatively modest computational resources. The model involving up to 11 million FDTD cells, requiring up to 1 GB RAM, and using 2-5 *s* heating time steps in the iterative solving of the coupled problem completes the simulation, on a Windows 10 workstation used in this study, within a few hours.

The reported EM-thermal coupled model is open for further development to serve in ongoing support of the system design aiming to ease the related experimental studies. A feature worth computationally studying is the effect of oblique incidence of the MMW field on temperature profiles and efficiency of absorption. Another important scenario is the

block without thermal insulation. Of a particular interest is a practical operational regime of a MMW HX in which some high temperature (reached through MMW heating of the susceptor and heat transfer to the metal baseplate) is locked and maintained constant to avoid overheating through a thermal sink and thus support the non-stop operation of the device. The latter problems can be addressed through manipulations with appropriate thermal boundary conditions.

References

Ayappa, K.G., Davis, H.T., Davis, E.A. and Gordon, J. (1991), "Analysis of microwave heating of materials with temperature-dependent properties", *AIChE Journal*, Vol. 37 No. 3, pp. 313-322.

Celuch, M. and Kopyt, P. (2009), "Modeling of microwave heating of foods", in Lorence, M.W. and Pesheck, P.S. (Eds), *Development of Packaging and Products for Use in Microwave Ovens*, Woodhead Publishing, pp. 305-348.

COMSOL Multiphyscis™ (1998-2019), v. 5.4, COMSOL AB, available at: www.comsol.com

Datta, A. and Anartheswaran, R.C. (2001), *Handbook of Microwave Technology for Food Application*, Marcel Dekker, New York, NY.

Etinger, A., Pilossof, M., Litvak, B., Hardon, D., Einat, M., Kapilevich, B. and Pinhasi, Y. (2017), "Characterization of a Shottky diode rectanna for millimeter wave power beaming using high power radiation sources", *Acta Physica Polonica A*, Vol. 131 No. 5, pp. 1280-1284.

Feher, L.E. (2009), *Energy Efficient Microwave Systems: Materials Processing Technologies for Avionic, Mobility and Environmental Applications*, Springer-Verlag, Berlin.

Gaone, J.M., Tilley, B.S. and Yakovlev, V.V. (2019), "Electromagnetic heating control via high-frequency resonance of a triple-layer laminate", *Journal of Engineering Mathematics*, Vol. 114 No. 1, pp. 65-86.

Hilario, M.S., Hoff, B.W., Jawdat, B.I., Dynys, F.W. and Wang, J.J. (2017), "High temperature millimeter-wave permittivity measurement setup for beamed energy heat exchangers", *55th AIAA Aerospace Sciences Meeting, 2017*, doi: 10.2514/6.2017-1340.

Hilario, M.S., Hoff, B.W., Jawdat, B., Lanagan, M.T., Cohick, A.W., Dynys, F.W., Mackey, J.A. and Gaone, J.M. (2019), "W-band complex permittivity measurements at high temperature using free-space methods", *IEEE Transactions on Components, Packaging and Manufacturing Technology*, Vol. 9 No. 6, pp. 1011-1019.

Hoff, B.W., Dynys, F.W., Hayden, S.C., Grudt, R.O., Hilario, M.S., Baros, A.E. and Ostraat, M.L. (2019a), "Characterization of AlN-based ceramic composites for use as millimeter wave susceptor materials at high temperature: high temperature thermal properties of AlN:Mo with 0.25% to 4.0% Mo by volume", *MRS Advances*, pp. 1-12, doi: 10.1557/adv.2019.142.

Hoff, B.W., Hayden, S.C., Hilario, M.S., Grudt, R.O., Dynys, F.W., Baros, A.E., Rittersdorf, I.M. and Ostraat, M.W. (2019b), "Characterization of AlN-based ceramic composites for use as millimeter wave susceptor materials at high temperature: dielectric properties of AlN:Mo with 0.25 v% to 4.0 v% Mo at temperatures from 25-550°C", *Journal of Materials Research*, Vol. 34 No. 15, pp. 2573-2581.

Hoff, B.W., Hilario, M.S., Jawdat, B., Baros, A.E., Dynys, F.W., Mackey, J.A., Yakovlev, V.V., Andraka, C.E., Armijo, K.M., Savrun, E. and Rittersdort, I.M. (2018), "Millimeter wave interactions with high temperature materials and their applications to power beaming", *Proc. 52nd IMPI Microwave Power Symp.*, Long Beach, CA, June 2018, pp. 82-83.

Hossan, M.R. and Dutta, P. (2012), "Effects of temperature dependent properties in electromagnetic heating", *International Journal of Heat and Mass Transfer*, Vol. 55 Nos 13/14, pp. 3412-3422.

Jamar, A., Majid, Z.A.A., Azmi, W.H., Norhafana, M. and Razak, A.A. (2016), "A review of water heating system for solar energy applications", *International Communications in Heat and Mass Transfer*, Vol. 76, pp. 178-187.

Jawdat, B., Hoff, B., Hilario, M., Baros, A., Pelletier, P., Sabo, T. and Dynys, F. (2017), "Composite ceramics for power beaming", *Proc. 2017 IEEE Wireless Power Transfer Conf.*, 978-1-5090-4595-3/17.

Kashimura, K., Sugawara, H., Hayashi, M., Mitani, T. and Shinohara, N. (2016), "Microwave heating behavior and microwave absorption properties of barium titanate at high temperatures", *AIP Advances*, Vol. 6 No. 6, p. 065001.

Komerath, N. and Kar, A. (2012), "Retail beamed power using millimeter waves: survey", *ACM Journal on Emerging Technologies in Computing Systems*, Vol. 8 No. 3, pp. 18:1-18:25.

Komurasaki, K. and Tabata, K. (2018), "Development of a novel launch system microwave rocket powered by millimeter-wave discharge", *International Journal of Aerospace Engineering*, Vol. 2018, doi: 10.1155/2018/9247429, 9 pages.

Kopyt, P. and Celuch, M. (2007), "Coupled electromagnetic-thermodynamic simulations of microwave heating problems using the FDTD algorithm", *Journal of Microwave Power and Electromagnetic Energy*, Vol. 41 No. 4, pp. 18-29.

Koutchma, T. and Yakovlev, V.V. (2010), "Computer modeling of microwave heating processes for food preservation", in Farid, M. (Ed.), *Mathematical Analysis of Food Processing*, CRC Press, Boca Raton, FL, pp. 625-657.

Kumi, P. and Yakovlev, V.V. (2019), "Computational procedure for quantitative characterization of uniformity of high frequency heating", *Proc. of 53th IMPI's Microwave Power Symp*, Las Vegas,, June 2019, pp. 123-125.

Langer, P., Maeder, M., Guist, C., Krause, M. and Marburg, S. (2017), "More than size elements per wavelength: the practical use of structural finite element models and their accuracy in comparison with experimental results", *Journal of Computational Acoustics*, Vol. 25 No. 4, p. 1750025.

Leadbeater, N. (2010), *Microwave Heating as a Tool for Sustainable Chemistry*, CRC Press, Boca Raton, FL.

Mohekar, A.A., Gaone, J.M., Tilley, B.S. and Yakovlev, V.V. (2018a), "A 2D coupled electromagnetic, thermal and fluid flow model: application to layered microwave heat exchangers", In *IEEE MTT-S Intern. Microwave Symp. Dig.*, Philadelphia, PA, June 2018, pp. 1389-1392.

Mohekar, A.A., Gaone, J.M., Tilley, B.S. and Yakovlev, V.V. (2018b), "Multiphysics simulation of temperature profiles in a triple-layer model of a microwave heat exchanger", *Proc. 52nd IMPI's Microwave Power Symp.*, Long Beach, CA, June 2018, pp. 33-35.

Mohekar, A.A., Tilley, B.S. and Yakovlev, V.V. (2019a), "A 2D model of a triple layer electromagnetic heat exchanger with porous media flow", *IEEE MTT-S Intern. Microwave Symp. Dig.*, Boston, MA, June 2019, p. 4.

Mohekar, A.A., Tilley, B.S. and Yakovlev, V.V. (2019b), "Plane wave irradiation of a layered system: resonance-based control over thermal runaway", *Proc. 17th Intern. Conf. on Microwave and High Frequency Heating (AMPERE 2019)*, Valencia, September 2019, pp. 292-311.

Moon, E.M. and Yakovlev, V.V. (2018), "Computer-aided design of a dielectric insert supporting uniformity of fast microwave heating", *COMPEL – the International Journal for Computation and Mathematics in Electrical and Electronic Engineering*, Vol. 36 No. 6, pp. 1958-1968.

Mur, G. (1981), "Absorbing boundary conditions for the finite-difference approximation of the time-domain electromagnetic-field equations", *IEEE Transactions on Electromagnetic Compatibility*, Vol. 23 No. 11, pp. 377-382.

Parkin, K.L., DiDomenico, L.D. and Culick, F.E. (2004), "The microwave thermal thruster concept", *2nd Intern. Symp. on Beamed Energy Propulsion*, pp. 418-429, 0-7354-0175-6/04.

QuickWave™ (1998-2019), v. 2018, QWED Sp. z o. o., available at: www.qwed.eu

Salvi, D.A., Boldor, D., Aita, G.M. and Sabliov, C.M. (2011), "COMSOL multiphysics model for continuous flow microwave heating of liquids", *Journal of Food Engineering*, Vol. 104 No. 3, pp. 422-429.

Salvi, D.A., Boldor, D., Ortego, J., Aita, G.M. and Sabliov, C.M. (2010), "Numerical modeling of continuous flow microwave heating: a critical comparison of COMSOL and ANSYS", *J. of Microwave Power and Electromag. Energy*, Vol. 44 No. 4, pp. 187-197.

Willert-Porada, M. (2006), *Advances in Microwave and Radio Frequency Processing*, Springer-Verlag, Berlin.

Yakovlev, V.V., Allan, S.M., Fall, M.L. and Shulman, H.S. (2011), "Computational study of thermal runaway in microwave processing of zirconia", in Tao, J. (Ed.), *Microwave and RF Power Applications*, Cépaduès Éditions, Toulouse, pp. 303-306.

Yu, W. (2009), *Electromagnetic Simulation Techniques Based on the FDTD Method*, Wiley, Hoboken, NJ.

Corresponding author
Vadim V. Yakovlev can be contacted at: vadim@wpi.edu